



Microstructural evolution and mechanical properties of laser melting deposited Ti–6.5Al–3.5Mo–1.5Zr–0.3Si titanium alloy

Hai-shui REN, Xiang-jun TIAN, Dong LIU, Jian LIU, Hua-ming WANG

Laboratory of Laser Materials Processing and Manufacturing, Beihang University, Beijing 100191, China

Received 13 August 2014; accepted 30 December 2014

Abstract: A rectangular plate of Ti–6.5Al–3.5Mo–1.5Zr–0.3Si titanium alloy was fabricated by laser melting deposition (LMD) technology. Macrostructure and microstructure were characterized by optical microscope (OM) and scanning electron microscope (SEM). Room temperature tensile properties were evaluated. Results indicate that the macro-morphology is dominated by large columnar grains traversing multiple deposited layers. Two kinds of bands, named the wide bands and the narrow bands, are observed. The wide band consists of crab-like α lath and Widmanstätten α colony. The narrow band consists of α lath and transformed β . The formation mechanism of the two bands was explored. The influence of heat effect caused by subsequent deposition layers on microstructural evolution during deposition process was discussed. The room temperature tensile test demonstrates that the strength of laser deposited Ti–6.5Al–3.5Mo–1.5Zr–0.3Si is comparable to that of wrought bars.

Key words: titanium alloy; microstructure; tensile properties; laser melting deposition

1 Introduction

Laser melting deposition (LMD) manufacturing technology, a newly developed fabrication technology that combines the prototyping and laser cladding techniques, can fabricate fully dense, high performance and complex shaped metal components without using any molds [1]. The technology is also known as laser engineered net shaping (LENS) [2], direct light fabrication (DLF) [3], direct metal deposition (DMD) [4], laser additive manufacturing (LAM) [5] and selective laser melting (SLM) [6]. Compared with conventional manufacturing technologies, LMD offers many outstanding advantages, such as shorter design-to-production cycle, lower cost, higher utilization ratio of material. It is worthwhile to point out that LMD enables the fabrication of near-net-shape metallic components with complex geometric shapes or graded microstructure/composition. Hence, LMD technology is especially suitable to manufacture large titanium alloy components which are difficult to fabricate by traditional wrought-based process.

Actually, plenty of researchers have focused on the fabrication of titanium alloys by LMD technology

[7–16]. In Ref. [7], Ti–6Al–4V was manufactured by direct light fabrication (DLF) technology and the influences of processing parameters on microstructure were studied. The layer bands which consisted of coarse α and β laths were found in the heat affected zone below the interface between adjacent layers. KELLY and KAMPE [9] fabricated Ti–6Al–4V builds through laser additive manufacturing (LAM) process, and the mechanism of microstructural evolution and the forming process of layer bands were explored. In another study, TIAN et al [10] created a Ti–4Al–1.5Mo plate by LMD and the effects of annealing temperatures on microstructure and impact toughness were analyzed. In studies of BAUFELD et al [12,13], several components were deposited by shaped metal deposition (SMD) and two kinds of bands, i.e., parallel bands and convex bands, were observed. Moreover, AHSAN et al [15] discussed the effects of laser powers and mass flows of powders on prior beta grains of Ti–6Al–4V fabricated by laser direct metal deposition (LDMD). In a recent paper [16], a graded structural material (GSM) of Ti–6Al–4V/Ti–6.5Al–3.5Mo–1.5Zr–0.3Si was manufactured by LMD, and a columnar-to-equiaxed-to-columnar transition of grains and the thermal behavior of molten pool during LMD process were analyzed.

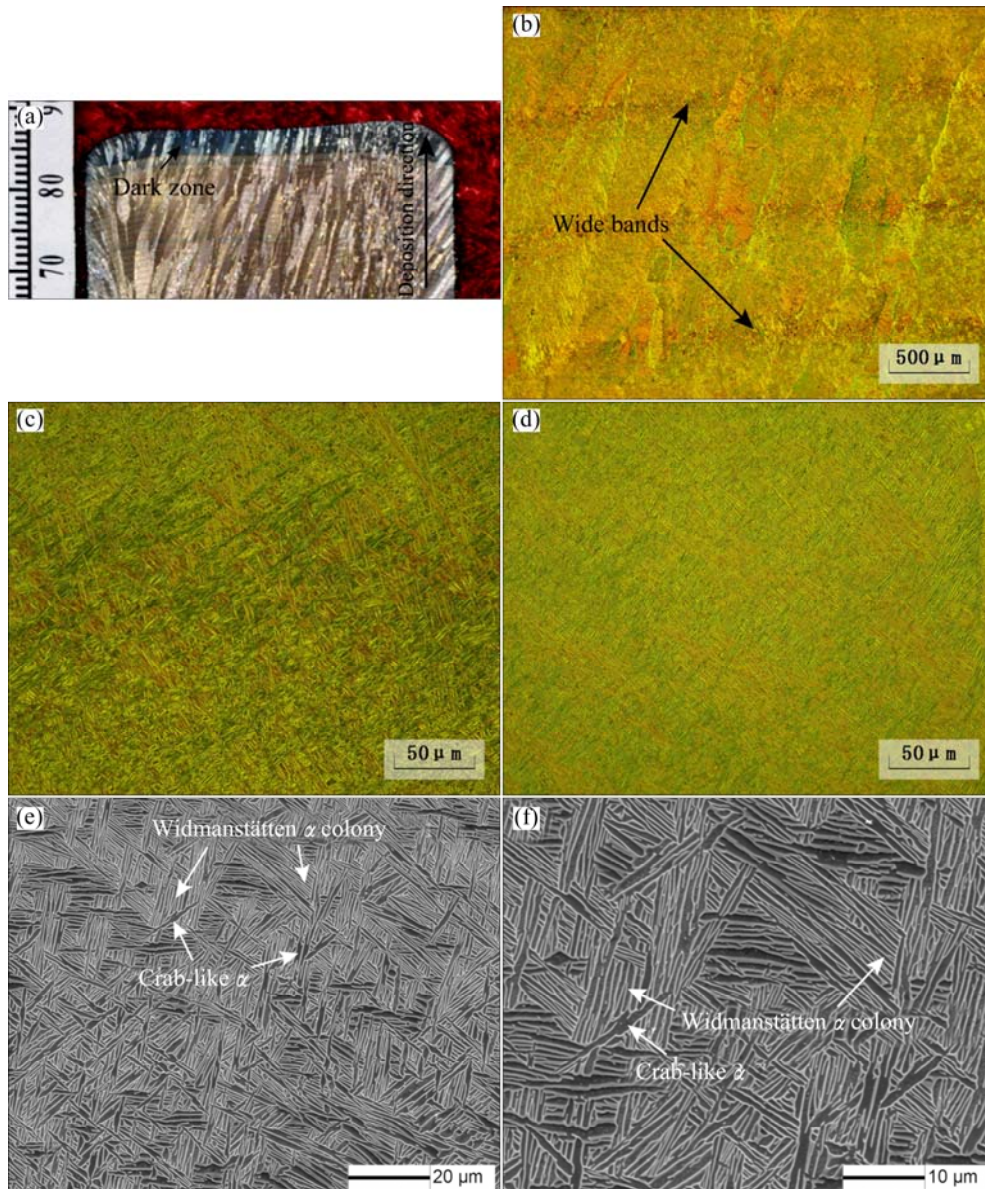


Fig. 3 Morphologies of laser deposited Ti-6.5Al-3.5Mo-1.5Zr-0.3Si plate on YOZ section: (a) Macro-morphology; (b) Locally magnified of (a); (c) Microstructure within wide band; (d) Nominal microstructure; (e) SEM morphology within wide band; (f) Locally magnified of (e)

laser deposited Ti-6.5Al-3.5Mo-1.5Zr-0.3Si plate on the YOZ section. As can be seen, no pores and fusion defects are present; and the sample is dominated by large columnar grains traversing multiple deposited layers. Several bands, called “wide bands”, are found as shown in Fig. 3(b). These wide bands are parallel and the width of a single one is 120–160 μm . The distance between the two adjacent wide bands is 700 μm approximately. Figure 3(c) presents the microstructure within a wide band. Compared with nominal microstructure (Fig. 3(d)) consisting of basketweave α laths, the microstructure in Fig. 3(c) is relatively coarse. For further analysis, the microstructure within the wide band is depicted by SEM as shown in Figs. 3(e) and (f). It can be seen that the

wide band consists of crab-like α and Widmanstätten α colony. The crab-like α is the α lath with tentacles on the end faces. And the volume fraction of crab-like α decreases gradually from the bottom to the top in Fig. 3(e). The Widmanstätten α colony is composed of several α laths with similarly aligned patterns (Fig. 3(f)).

Figure 4 displays the macro-morphology on the top area of the Ti-6.5Al-3.5Mo-1.5Zr-0.3Si plate. It is observed on the XOZ section on which tracks are overlapped with each other. A lot of deposited layers could be found and the last eight layers are marked by A-H, respectively. The thickness of each layer, except for the last deposited layer A, is about 764 μm corresponding to the distance between two adjacent wide

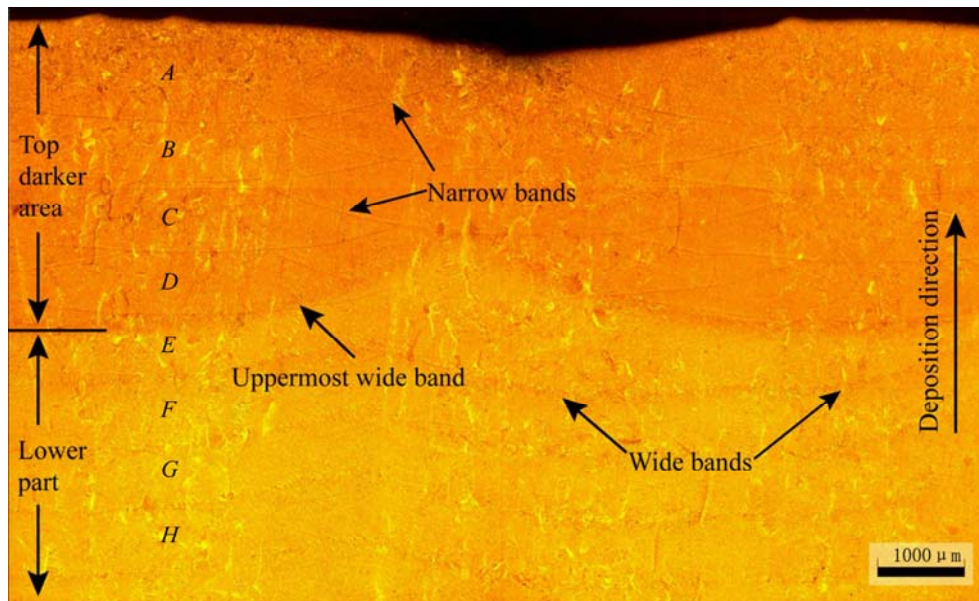


Fig. 4 Macro-morphology of laser deposited Ti-6.5Al-3.5Mo-1.5Zr-0.3Si plate on XOZ section

bands. The top darker area in Fig. 4 corresponds to the dark zone as marked by an arrow in Fig. 3(a). Wide bands and another kind of bands, named “narrow bands”, are visible in Fig. 4. The width of a single narrow band is much smaller than that of the wide band. The wide bands only appear in the lower part. In contrast, the narrow bands are present in the whole plate but difficult to be discerned in the lower part. Figure 5 illustrates the morphology of the dividing area between the darker area and the lower part in Fig. 4. A wide band and a narrow band are observed in this figure. This wide band is the uppermost one in the whole plate. In other words, wide bands are formed in the bottom of the darker area. Systematic variation in composition between and within bands did not exist as determined using the electron microprobe [9,20]. Hence, it could be proposed that the heat effect caused by subsequent deposition layers should take responsibility for the formations of bands.

3.2 Wide band

To explore the formation mechanism of the wide bands, the microstructure of last eight layers are studied. Figure 6(a) shows the solidification microstructure of layer A and Figs. 6(b)–(h) show the microstructures of layers B–H experienced heat effect caused by the depositions of subsequent layers above them. As shown in Fig. 6, the morphologies of layers A–D are similar and consist of ultra-fine α laths and transformed β . The heat effect with high cooling rate and peak heating temperature acting on layers B–D inhibit the growth of α phase. The width of α laths increases and the aspect ratio of α laths decreases in Fig. 6(e) compared with those in Figs. 6(a)–(d). Furthermore, the area fraction of α phase

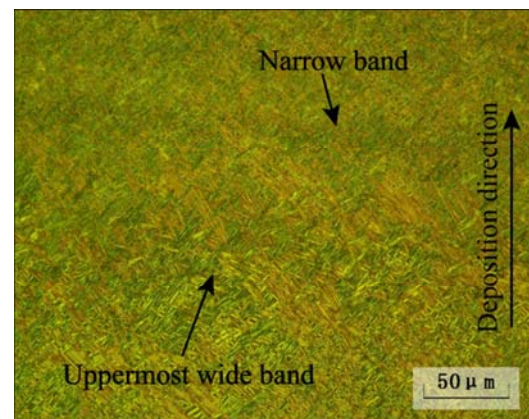


Fig. 5 Morphology of dividing area between darker area and lower part

has significantly increased and transformed β surrounded by α laths is observed as shown in Fig. 6(e). Due to the heat effect with low cooling rate and peaking heating temperature, α phase has further precipitated from β phase in layer E. Figure 6(f) shows the resulting microstructure morphology of layer F. Compared with Fig. 6(e), α laths continue coarsening and the volume fraction of α phase relatively increases. The transformed β surrounded by α laths still could be found, illustrating that α phase has not precipitated from β phase at the most extent. However, the transformed β has disappeared in the resulting microstructure of layer G (Fig. 6(g)), which demonstrates that α phase has precipitated sufficiently. Through comparing Fig. 6(g) with Fig. 6(h), it is indicated that there is no obvious difference in microstructure between layers G and H. In other words, the heat effect, which is caused by the deposition of layer

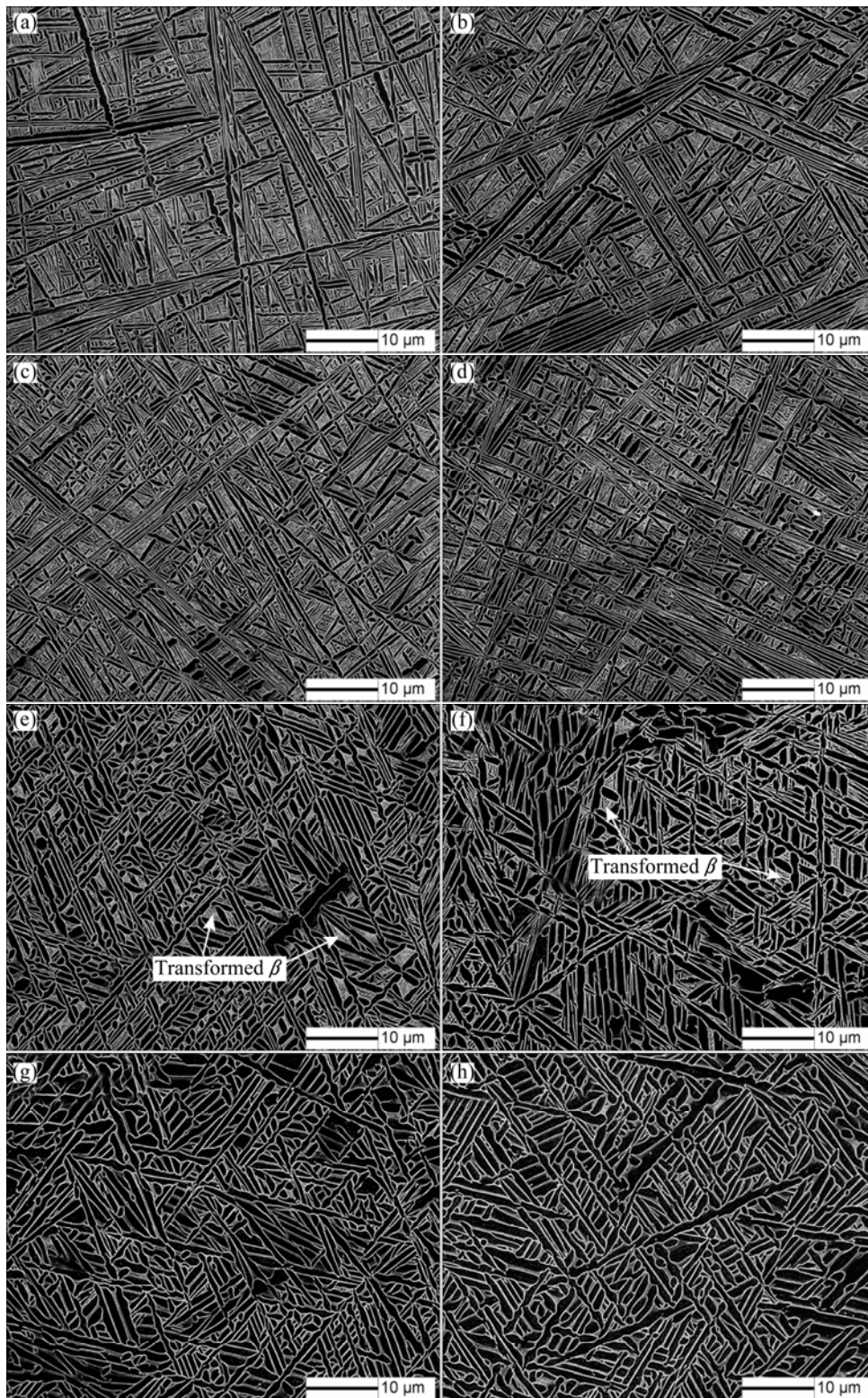


Fig. 6 Microstructures of last eight deposited layers *A–H* in Fig. 4: (a) Layer *A*; (b) Layer *B*; (c) Layer *C*; (d) Layer *D*; (e) Layer *E*; (f) Layer *F*; (g) Layer *G*; (h) Layer *H*

A, on layer *H* becomes useless. Hence, it is concluded that the microstructure in a layer has become stabilized after six layers deposited on it.

When a layer is deposited, a series of isotherms lines will form in the as-deposited part. According to the

significant differences in microstructure between Figs. 6(e)–(f) and Figs. 6(b)–(d), it is inferred that layers *B*, *C* and *D* experience a heat treatment with a temperature above β -transition point; layers *E*, *F*, *G* and *H* undergo a heat treatment with a temperature below

β -transition point as layer *A* is deposited. Based on the analysis and the morphology of Fig. 4, it is deduced that β -transition point is located in the dividing area between the darker area and the lower part. Therefore, according to Fig. 5, the wide band is formed in the position where the temperature is close to the β -transition point. As Fig. 3(e) illustrates, the crab-like α laths decrease gradually from the bottom to the top and disappear finally on the top. On the basis of the studies in Ref. [21], the crab-like α laths were obtained through heat treatments in the upper part of $\alpha+\beta$ phase region. Therefore, it is deduced that the wide band forms in the region below and closest to the β -transition point.

When layer *A* is deposited on layer *B* in Fig. 4, the region where the uppermost wide band forms is heated into a temperature very close to the β -transition point. Thus, only a few of α laths (denoted as pre-existing α laths) are retained. When temperature lowers, the pre-existing α laths grow and the morphology of crab-like α forms due to the preferential epitaxial growth of secondary α on the edge of pre-existing α laths along with the $\langle 1\bar{2}10 \rangle$ preferred crystallographic direction [21]. On the other hand, because α phase (HCP) and β phase (BCC) differ continuously and significantly in composition, the solute diffusion to and from the interface (denoted as α/β interface) between the pre-existing α lath and the parent β phase always occurs during the growth of the pre-existing α lath, which causes a supersaturation within β phase adjacent to the α/β interface [22,23]. The supersaturation will provide a chemical thermodynamic driving force for sympathetic nucleation. Sympathetic nucleation is defined as the nucleation of a precipitate crystal, which differs in composition from that of the matrix, at the inter-phase boundary of another crystal of the same phase [24]. This type of nucleation has been observed to occur frequently in Ti-based [25–27] and Fe-based [25,28] alloys. In the present work, the Widmanstätten α laths sympathetically nucleate in the vicinity of the broad face of the pre-existing α laths [22]. The nuclei which reach up to the critical radius before being over-run by the progression of the α/β interface could grow and spread into β phase rapidly [29]. Eventually, the Widmanstätten α laths impinge to other Widmanstätten α colony or crab-like α laths and the wide band forms. This formation mechanism of the Widmanstätten α colony has been discussed in our early work [30]. Through comparing the two wide bands in Fig. 3(c) and Fig. 5, it is known that the heat effect with a temperature below β -transition point has no obvious influences on the formed wide bands.

Actually, there is another mechanism, an unstable interface mechanism, about the formation of Widmanstätten plate. The thermal and solute gradients

and interfacial energy could lead to the perturbation of α/β interface [31,32]. When a protuberance emerges on the interface due to the perturbation and reaches a critical dimension, it could grow into β phase rapidly [29], forming Widmanstätten morphology. However, in this condition, the Widmanstätten α lath and pre-existing α lath should be monolithic due to no nucleation. In other words, there is no interface between the Widmanstätten α lath and pre-existing α lath and they should be connected to each other. Nevertheless, the interfaces occur universally in Fig. 3(f). Hence, the probability that Widmanstätten α colony within the wide band is resulted from the unstable interface mechanism is eliminated.

3.3 Narrow band

With regard to the narrow bands as shown in Fig. 5, they are difficult to be distinguished at high magnification. As Fig. 4 demonstrates, the narrow bands are clear in the top darker area but difficult to discern in the lower part. And the narrow bands are formed close to the bottom of the molting pool. Actually, the narrow bands are similar to the layer bands in Ref. [20] and the formation mechanism was discussed in detail. When a new layer is deposited on the previous material, a narrow solid region closest to the molten pool is heated into a very high temperature which is near the melting point. The high temperature reheating treatment results in high extent of homogenization within narrow band [20]. The microstructure exhibits a better corrosion resistance than that in other regions.

Generally, bands are a phenomenon observed frequently in the parts manufactured by deposition techniques, such as LMD and LAM. And a lot of studies about bands have been reported [7,9,12,13,20,33–36]. However, those analyses are unclear and disorderly. Many workers consider these two kinds of bands as one kind. Therefore, a summary based on previous and the present studies about bands has been proposed. Two kinds of bands, namely wide bands and narrow bands in this work, are also visible in the parts fabricated by deposition techniques. The wide bands are the same as the convex bands in Refs. [12,13] and the layer bands in Refs. [9,36]. The narrow bands are the same as the parallel bands in Refs. [12, 13] and the layer bands in Refs. [15, 20]. Based on the discussion and analyses as above, it is known that the narrow band definitely forms in the narrow solid region closest to the melting pool. It could be retained in β phase field. And the narrow band occurs in the whole plate and is difficult to be discerned in the lower part and at high magnification. Adversely, the wide band will disappear when the temperature is above β -transition point, and it forms in the region closest to β -transition point. Moreover, it is uncertain where the wide band appears in a layer. It is related to the

processing parameters, especially laser power, layer thickness, scanning strategy and the deposited materials. In sum, the narrow band and the wide band are two different kinds of bands. There is no relationship between the formation mechanisms of them. They should be studied separately.

3.4 Mechanical properties

Microhardness on and off a wide band is measured to determine whether the difference between the wide band and normal microstructure gives rise to a non-uniformity in mechanical properties. The microhardness curve across the wide band is shown in Fig. 7. As the curve illustrates, no evident differences in microhardness are found when the microhardness curve passes the wide band from normal region which is consistent with the result in Ref. [9].

The results of room temperature tensile test of laser deposited Ti–6.5Al–3.5Mo–1.5Zr–0.3Si titanium alloy are listed in Table 1. The ultimate tensile strength (UTS) and yield strength (YS) are comparable to those of wrought bars. However, the elongation (EL) and the reduction in area (RA) are only 56.7% and 37.8% of those of wrought bars, respectively. Figure 8 presents the fracture surfaces of the LMD specimens after room temperature tensile test. As Fig. 8(a) illustrates, the fracture mode is a mixture of transgranular failure and intergranular failure. Secondary cracks (indicated by

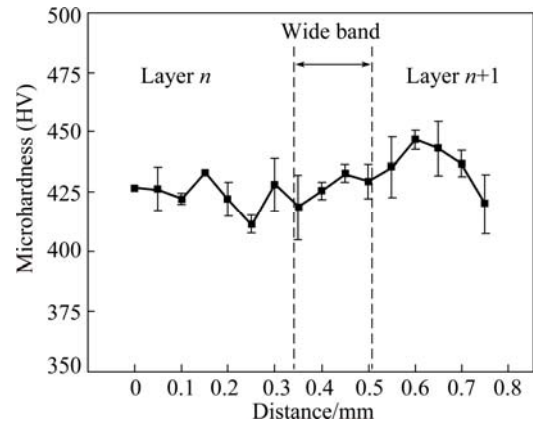


Fig. 7 Microhardness profile on and off wide band

Table 1 Room temperature tensile properties of laser deposited Ti–6.5Al–3.5Mo–1.5Zr–0.3Si titanium alloy

Material	UTS/MPa	YS/MPa	EL/%	RA/%
Laser deposited	1101±9	1030±11	10.2±2.2	17±1
Wrought bar (950 °C, 1 h, AC+ 530 °C, 6 h, AC) [17]	1119	998	18	45

arrows in Figs. 8(a) and (b)), steps (Figs. 8(b) and (c)) and inter-granular fracture characteristics (Fig. 8(d)) are found. Shallow dimples are observed at the top of the steps (Fig. 8(c)). However, the dimples disappear and the

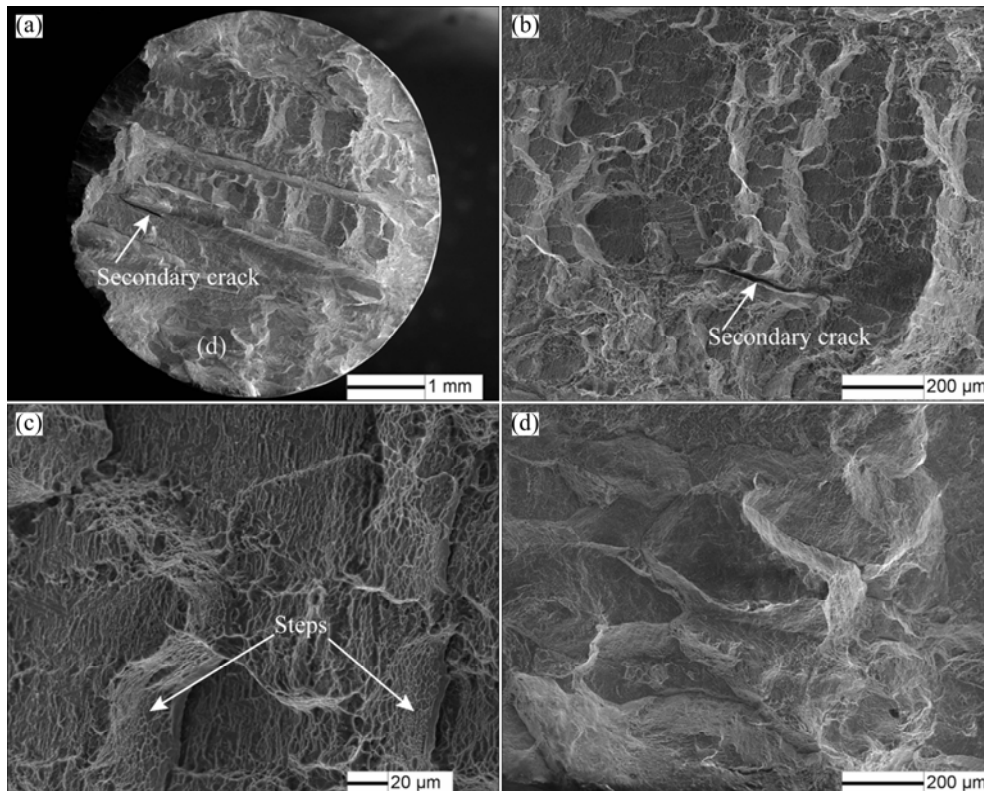


Fig. 8 Fracture morphologies of room temperature tensile specimen: (a) Overall view; (b) Steps; (c) High magnification of steps; (d) Inter-granular fracture characteristics

secondary cracks are visible at the bottom of the steps. The step might be resulted from the intersection of two cracks propagating in different crystallographic planes. Short interruption occurs at the bottom of the step in the intersecting moment. The formation of steps increases the crack propagation path and more energy is absorbed.

As shown in Fig. 3(a), the sample is dominated by large columnar grains. A large amount of grain boundaries exist in the specimens for room temperature tensile test and their orientations are perpendicular to the loading direction due to the principle axis of the specimens perpendicular to the building direction. This is detrimental to the plasticity [13,37]. Hence, the specimens present a poor tensile ductility.

4 Conclusions

1) The influence of heat effect caused by subsequent deposition layers on microstructural evolution during laser melting deposition process was discussed. Microstructure in a certain layer could be stabilized after six subsequent layers are deposited on the layer.

2) Two kinds of bands, namely narrow bands and wide bands, were found. The narrow band consisted of α lath and transformed β . It formed in the narrow solid region closest to the melting pool. The wide band was composed of crab-like α laths and Widmanstätten α colony. It formed in the region closest to β -transition point.

3) The tensile strengths of laser deposited Ti-6.5Al-3.5Mo-1.5Zr-0.3Si titanium alloy were comparable to those of the wrought bar. The ductility was relatively poor due to the large number of grain boundaries and their orientation perpendicular to the loading direction.

References

- [1] DONG Li-xin, WANG Hua-ming. Microstructure and mechanical properties of laser melting deposited $Ti_2Ni_3Si/NiTi$ Laves alloy [J]. Transactions of Nonferrous Metals Society of China, 2007, 17(6): 1230–1235.
- [2] HOMEISTER W, GRIFFITH M, ENSZ M, SMUGERESKY J. Solidification in direct metal deposition by LENS processing [J]. JOM Journal of the Minerals Metals and Materials Society, 2001, 53: 30–34.
- [3] MILEWSKI J O, LEWIS G K, THOMA D J, KEEL G I, NEMEC R B, REINERT R A. Directed light fabrication of a solid metal hemisphere using 5-axis powder deposition [J]. Journal of Materials Processing Technology, 1998, 75: 165–172.
- [4] MAZUMDER J, DUTTA D, KIKUCHI N, GHOSH A. Closed loop direct metal deposition: Art to part [J]. Optics and Lasers in Engineering, 2000, 34: 397–414.
- [5] ARCELLA F G, FROES F H. Producing titanium aerospace components from powder using laser forming [J]. JOM Journal of the Minerals Metals and Materials Society, 2000, 52: 28–30.
- [6] MURR L E, GAYTAN S M, RAMIREZ D A, MARTINEZ E, HERNANDEZ J, AMATO K N, SHINDO P W, MEDINA F R, WICHER R B. Metal fabrication by additive manufacturing using laser and electron beam melting technologies [J]. Journal of Materials Science and Technology, 2012, 28: 1–14.
- [7] WU Xin-hua, LIANG Jing, MEI Jun-fa, MITCHELL C, GOODWIN P S, VOICE W. Microstructures of laser-deposited Ti-6Al-4V [J]. Materials and Design, 2004, 25: 137–144.
- [8] LI Zhen, TIAN Xiang-jun, TANG Hai-bo, WANG Hua-ming. Low cycle fatigue behavior of laser melting deposited TC18 titanium alloy [J]. Transactions of Nonferrous Metals Society of China, 2013, 23(9): 2591–2597.
- [9] KELLY S M, KAMPE S L. Microstructural evolution in laser-deposited multilayer Ti-6Al-4V builds: Part I Microstructural characterization [J]. Metallurgical and Materials Transactions A, 2004, 35: 1861–1867.
- [10] TIAN X J, ZHANG S Q, LI A, WANG H M. Effect of annealing temperature on the notch impact toughness of a laser melting deposited titanium alloy Ti-4Al-1.5Mn [J]. Materials Science and Engineering A, 2010, 527: 1821–1827.
- [11] QIAN Ting-ting, LIU Dong, TIAN Xiang-jun, LIU Chang-meng, WANG Hua-ming. Microstructure of TA2/TA15 graded structural material by laser additive manufacturing process [J]. Transactions of Nonferrous Metals Society of China, 2014, 24: 2729–2736.
- [12] BAUFELD B, van der BIEST O, GAULT R. Microstructure of Ti-6Al-4V specimens produced by shaped metal deposition [J]. International Journal of Materials Research, 2009, 100: 1536–1542.
- [13] BAUFELD B, van der BIEST O, GAULT R. Additive manufacturing of Ti-6Al-4V components by shaped metal deposition: Microstructure and mechanical properties [J]. Materials and Design, 2010, 31(S): s106–s111.
- [14] ZHANG A-li, LIU Dong, TANG Hai-bo, WANG Hua-ming. Microstructure evolution of laser deposited Ti60A titanium alloy during cyclic thermal exposure [J]. Transactions of Nonferrous Metals Society of China, 2013, 23(11): 3249–3256.
- [15] AHSAN M N, PINKERTON A J, MOAT R J, SHACKLETON J. A comparative study of laser direct metal deposition characteristics using gas and plasma-atomized Ti-6Al-4V powders [J]. Materials Science and Engineering A, 2011, 528: 7648–7657.
- [16] REN H S, LIU D, TANG H B, TIAN X J, ZHU Y Y, WANG H M. Microstructure and mechanical properties of a graded structural material [J]. Materials Science and Engineering A, 2014, 611: 362–369.
- [17] Beijing Institute of Aeronautical Materials. Materials databook for the design of aero-engines [M]. Beijing: China National Aero-Engine Corporation, 1989.
- [18] LONG Ri-sheng, LIU Wei-jun, XING Fei, WANG Hua-bing. Numerical simulation of thermal behavior during laser metal deposition shaping [J]. Transactions of Nonferrous Metals Society of China, 2008, 18: 691–699.
- [19] LIU Wei-ping, DUPONT J N. In-situ reactive processing of nickel aluminides by laser-engineered net shaping [J]. Metallurgical and Materials Transactions A, 2003, 34: 2633–2641.
- [20] LIU C M, TIAN X J, TANG H B, WANG H M. Microstructural characterization of laser melting deposited Ti-5Al-5Mo-5V-1Cr-1Fe near β titanium alloy [J]. Journal of Alloys and Compounds, 2013, 572: 17–24.
- [21] LU Y, TANG H B, FANG Y L, LIU D, WANG H M. Microstructure evolution of sub-critical annealed laser deposited Ti-6Al-4V alloy [J]. Materials and Design, 2012, 37: 56–63.
- [22] AARONSON H I, SPANOS G, MASAMURA R A, VARDIMAN R G, MOON D W, MENON E S K, HALL M G. Sympathetic nucleation: An overview [J]. Materials Science and Engineering B, 1995, 32: 107–123.

- [23] PHELAN D, DIPPENAAR R. Widmanstätten ferrite plate formation in low-carbon steels [J]. Metallurgical and Materials Transactions A, 2004, 35: 3701–3706.
- [24] MENON E S K, AARONSON H I. Overview no. 57 morphology, crystallography and kinetics of sympathetic nucleation [J]. Acta Metallurgica, 1987, 35: 549–563.
- [25] ZACKAY V F, AARONSON H I. Decomposition of austenite by diffusional processes [M]. New York: Interscience, 1962.
- [26] UNNIKRIISHNAN M, MENON E S K, BANERJEE S. Kinetics of alpha precipitation in Ti-6 wt % Cr and Ti-11 wt % Mo [J]. Journal of Materials Science, 1978, 13: 1401–1410.
- [27] MENON E S K, KRISHNAN R. Phase transformations in Ti-V alloys [J]. Journal of Materials Science, 1983, 18: 375–382.
- [28] RICKS R A, HOWELL P R, BARRITTE G S. The nature of acicular ferrite in HSLA steel weld metals [J]. Journal of Materials Science, 1982, 17: 732–740.
- [29] SUN Zhi-chao, GUO Shuang-shuang, YANG He. Nucleation and growth mechanism of α -lamellae of Ti alloy TA15 cooling from an $\alpha + \beta$ phase field [J]. Acta Materialia, 2013, 61: 2057–2064.
- [30] REN H S, TIAN X J, WANG H M. Effect of heat treatment on microstructure and mechanical properties of a graded structural material [J]. Materials Science and Engineering A, 2014, 614: 207–213.
- [31] MULLINS W W, SEKERKA R F. Morphological stability of a particle growing by diffusion or heat flow [J]. Journal of Applied Physics, 1963, 34: 323–329.
- [32] MULLINS W W, SEKERKA R F. Stability of a planar interface during solidification of a dilute binary alloy [J]. Journal of Applied Physics, 1964, 35: 444–451.
- [33] KOBRYN P A, SEMIATIN S L. The laser additive manufacture of Ti-6Al-4V [J]. JOM Journal of the Minerals Metals and Materials Society, 2001, 53: 40–42.
- [34] KOBRYN P A, MOORE E H, SEMIATIN S L. The effect of laser power and traverse speed on microstructure, porosity, and build height in laser-deposited Ti-6Al-4V [J]. Scripta Materialia, 2000, 43: 299–305.
- [35] KOBRYN P A, SEMIATIN S L. Microstructure and texture evolution during solidification processing of Ti-6Al-4V [J]. Journal of Materials Processing Technology, 2003, 135: 330–339.
- [36] BRANDL E, PALM F, MICHAILOV V, VIEHWEGER B, LEYENS C. Mechanical properties of additive manufactured titanium (Ti-6Al-4V) blocks deposited by a solid-state laser and wire [J]. Materials and Design, 2011, 32: 4665–4675.
- [37] BAUFELD B, van der BIEST O. Mechanical properties of Ti-6Al-4V specimens produced by shaped metal deposition [J]. Science and Technology of Advanced Materials, 2009, 10: 1–10.

激光熔化沉积 Ti-6.5Al-3.5Mo-1.5Zr-0.3Si 钛合金的组织演变与力学性能

任海水, 田象军, 刘 栋, 刘 健, 王华明

北京航空航天大学 激光材料制备与成形实验室, 北京 100191

摘 要: 利用激光熔化沉积技术制备 Ti-6.5Al-3.5Mo-1.5Zr-0.3Si 钛合金板材, 并采用金相和扫描电镜对合金的宏观组织和微观组织进行表征, 对室温拉伸性能进行研究。结果显示: 宏观形貌由贯穿多个沉积层的大柱状晶组成; 观察到宽条带和窄条带 2 种条带, 宽条带由 α 板条和魏氏集束构成, 窄条带由 α 板条和 β 转变组织构成, 对条带的形成机理进行探讨。此外, 还讨论由后续沉积层的沉积导致的热效应对组织演变的影响。室温拉伸测试显示, 激光熔化沉积制备的 Ti-6.5Al-3.5Mo-1.5Zr-0.3Si 钛合金的强度达到锻件强度水平。

关键词: 钛合金; 显微组织; 拉伸性能; 激光熔化沉积

(Edited by Yun-bin HE)